

# Controlling the interchain packing and photovoltaic properties via fluorine substitution in terpolymers based on benzo[1,2-c:4,5-c']dithiophene-4,8-dione and benzothiadiazole units

Gururaj P. Kini, Jun Young Choi, Sung Jae Jeon, Il Soon Suh, Doo Kyung Moon\*

*Nano and Information Materials (NIMs) Laboratory, Department of Chemical Engineering, Konkuk University, 120, Neungdong-ro, Gwangjin-gu, Seoul, 05029, South Korea*



## ARTICLE INFO

### Article history:

Received 13 April 2018

Received in revised form

7 June 2018

Accepted 12 June 2018

Available online 18 June 2018

### Keywords:

Polymer solar cells

Terpolymer

Fluorinated polymers

## ABSTRACT

We present a series of three terpolymers involving benzo [1,2-c:4,5-c']dithiophene-4,8-dione (BDD) and benzothiadiazole (BT) as acceptor units, and oligothiophene as the donor unit (PBDD-TnFBT terpolymers). We optimized the structures of these terpolymers by varying the number of fluorine (F) atoms on the BT unit and studied its effects on photovoltaic performance (**P1** (BT), **P2** (FBT), and **P3** (2FBT)). Density functional theory analysis, optical-electrochemical analysis, and X-ray diffraction study revealed that the fluorination of BT significantly decreased frontier energy levels, enhanced both intermolecular interactions and planarization of polymer backbone in the resulted polymers. As a result, **P3**, having two F substituents on BT, exhibited stronger intermolecular interactions, predominant face-on orientation with a shorter  $\pi$ - $\pi$  stacking distance of 3.51 Å, high hole mobility, and optimal nanoscale morphology compared to single F substituent (**P2**) and zero F substituent (**P1**) counterparts. Consequently, polymer solar cells based on **P3** demonstrated higher power conversion efficiency (PCE) of 6.2% than those based on **P1** and **P2** (1.4 and 1.7% respectively). This study illustrates the interrelation between the degree of fluorination and photovoltaic performance and effectively contributes to the design of high-PCE polymer donors for photovoltaic application.

© 2018 Elsevier Ltd. All rights reserved.

## 1. Introduction

Polymer solar cells (PSCs) are emerged as a prominent renewable energy source owing to their advantageous properties like solution processability, lightweight, and flexibility [1–5]. Recently, PSCs with bulk heterojunction (BHJ) structures have demonstrated a power conversion efficiency (PCE) of over 11% with fullerene [6–9] and 13% with non-fullerene acceptors [10–14], signifying their potential as portable power source. This dramatic rise in the PCE of PSCs is mainly due to the design and synthesis of high-performance donor materials by optimizing the structures of donor (D) and acceptor (A) units, controlling their nanoscale morphology, and improving device fabrication conditions.

The synthesis of conjugated polymers with a donor-acceptor (D-A) structure is an efficient and reliable approach to design polymers with a high PCE of over 10%. However, this method still lacks

precision control to simultaneously obtain deep highest occupied molecular orbital (HOMO) levels and broader absorption spectrum [15–17]. To overcome these drawbacks, a new class of polymers called terpolymers with three dissimilar monomeric units in the polymer backbone have been introduced (A<sub>1</sub>–D–A<sub>2</sub> or D<sub>1</sub>–A–D<sub>2</sub> type terpolymers) [17]. Through proper selection and optimization of the molar ratios of the three components, these terpolymers displayed advantages such as easy control of optical bandgap, lower energy levels, high carrier mobilities, control of miscibility, and solubility [17–24]. For example, Ma et al. designed and synthesized the terpolymer, PffBT2-DPPT2, with diketopyrrolopyrrole (DPP) and difluoro-benzothiadiazole (2FBT) as acceptor units and achieved PCEs of above 8.6% due to broader absorption range and deep HOMO levels [20]. Similarly, Lee and co-workers have reported a series of semi-crystalline terpolymers based on di-alkoxy benzothiadiazole (BTOR) and 2FBT, which exhibited PCEs of over 8% through the optimization of alkyl chain length and branching [23]. Furthermore, Huang et al. have reported the terpolymer, PTB7-Th-T2, which demonstrated an impressive PCE of 8.9% by incorporating a cheaper 2,2'-bithiophene as the third component into the PTB7-

\* Corresponding author.

E-mail address: [dkmoon@konkuk.ac.kr](mailto:dkmoon@konkuk.ac.kr) (D.K. Moon).

Th backbone [24]. Hence, terpolymer syntheses have emerged as a reliable strategy to design high-efficiency polymers for PSCs.

Motivated by these results, we designed and synthesized 5, 7-bis (dialkyl) benzo [1,2-c:4,5-c']-dithiophene-4,8-dione (BDD)- and benzothiadiazole (BT)-based terpolymers (PBDD-TnFBT), where BDD and BT are used as acceptors ( $A_1$  and  $A_2$ , respectively) and the spacer thiophene acts like a donor unit (D) (Scheme 1). Recently, the BDD acceptor core has been studied intensively in PSCs owing to its advantageous properties such as large planar structure, strong electron-withdrawing ability, and aggregation tendency, which lead to high PCE [25–30]. Moreover, drafting a suitable alkyl chain on the BDD ensures solubility and interchain packing in the resulting polymers [30]. However, most of the BDD-based polymers exhibited limited absorption range (~700 nm), which hinder the further enhancement of their PCEs with fullerene acceptor [26–30]. In response, we adopted an  $A_1$ -D- $A_2$  approach that broadens the absorption range via intramolecular charge transfer (ICT) interaction between the donor and two acceptor units [17,20,21,23]. The electron-deficient BT acceptor was selected as a second acceptor ( $A_2$ ) because of its structural versatility with 5- and 6-functionalizable positions. These can be easily substituted with different functional groups such as fluorine (F) [31–36], chlorine (Cl) [37–39], alkoxy (OR) [23,40], and nitrile (CN) [32,41], resulting in easy modulation of optoelectronic properties and intra/inter-chain properties of the resulting polymers. Particularly, adding electron-withdrawing F atoms to BT lowers the frontier energy levels (due to its strong electron-withdrawing nature) and enhances co-planarity and crystallinity (resulting from intra- and intermolecular non-covalent  $F\cdots S$  and  $C-H\cdots F$  columbic interactions) [31–36], thereby affecting the overall charge carrier mobility and PCE. Accordingly, we optimized the electronic properties, planarity, and intra/intermolecular interactions in our PBDD-TnFBT terpolymers by varying the number of F groups at the 5- and/or 6-position of the BT. At the same time, BDD with an appropriate alkyl chain was used to control the solubility of the resulting polymers. Thus, this design promises broader absorption, lower HOMO levels, and good solution processability.

We report three PBDD-TnFBT polymers having different numbers of F atoms, namely poly-{1,3-bis(2-octyldodecyl)-5-(5-(7-thiophen-2-yl)benzo [c] [1,2,5]thiadiazol-4-yl)thiophen-2-yl)-4H,8H-benzo [1,2-c:4,5-c']dithiophene-4,8-dione} (**P1**,  $n = 0$ ), poly-{5-(5-(5-fluoro-7-(thiophen-2-yl)benzo [c] [1,2,5]thiadiazol-4-yl)thiophen-2-yl)-1,3-bis(2-octyldodecyl)-4H, 8H-benzo [1,2-c:4,5-c']dithiophene-4,8-dione} (**P2**,  $n = 1$ ), and poly-{5-(5-(5,6-difluoro-7-(thiophen-2-yl)benzo [c] [1,2,5]thiadiazol-4-yl)thiophen-2-yl)-1,3-bis(2-octyldodecyl)-4H, 8H-benzo [1,2-c:4,5-c']dithiophene-4,8-dione} (**P3**,  $n = 2$ ). We studied the effect of fluorination on the optical, electrochemical, and photovoltaic properties of these

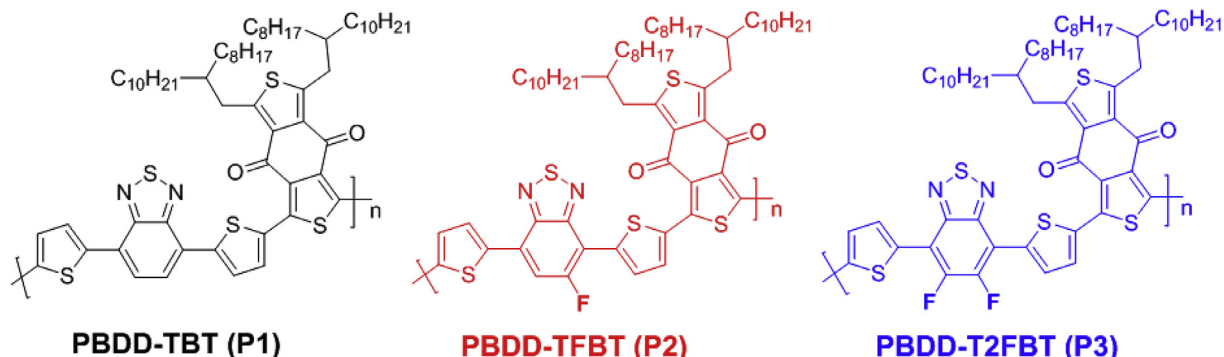
polymers. The PSCs fabricated with the fluorinated polymers (**P2** and **P3**) demonstrated higher PCEs of 1.7% and 6.2%, respectively, due to a higher open-circuit voltage ( $V_{OC}$ ) and short-circuit current density ( $J_{SC}$ ) than those of the non-fluorinated counterpart **P1** (PCE = 1.4%). We correlated the photovoltaic performances of the polymers with the degree of fluorination on the polymer backbone by evaluating DFT analysis, opto-electronic properties, X-ray diffraction (XRD), hole mobility, and nanoscale morphology of the resultant polymers. The detailed study on the effect of fluorination on the PBDD-TnFBT polymers are summarized below.

## 2. Results and discussion

### 2.1. Synthesis of polymers and thermal properties

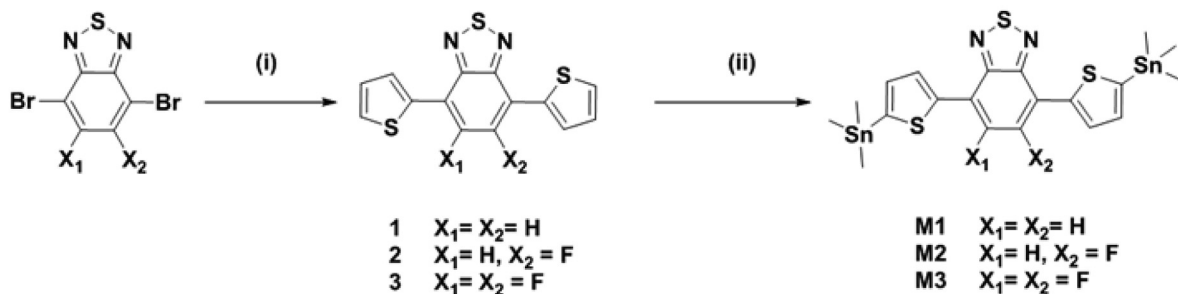
The synthesis of the monomers and polymers are shown in Scheme 2. The BT monomers 4,7-bis(5-(trimethylstannyl)thiophen-2-yl)benzo [c][1,2,5]thiadiazole (M1) [34] 5-fluoro-4,7-bis(5-(trimethylstannyl)thiophen-2-yl)benzo [c][1,2,5]thiadiazole (M2) [34] and 5,6-difluoro-4,7-bis(5-(trimethylstannyl)thiophen-2-yl)benzo [c][1,2,5]thiadiazole (M3) [34] were prepared according to previous reported procedures. The BDD monomer, 1,3-dibromo-5,7-bis(2-octyldodecyl)-4H, 8H-benzo [1,2-c:4,5-c']dithiophene-4,8-dione (M4), was synthesized by cyclization reaction between 2,5-bis(2-octyldodecyl)thiophene and 2,5-dibromothiophene-3,4-dicarbonyl dichloride in anhydrous aluminum chloride ( $AlCl_3$ ) [30]. 2-octyldodecyl chains were drafted on the BDD (M4) to ensure sufficient solubility of the resultant polymers for solution processing. Finally, polymers **P1**, **P2**, and **P3** were synthesized through the microwave-assisted Stille coupling reaction between the corresponding monomers in the presence of tris(dibenzylideneacetone)dipalladium (0) ( $Pd(dbu)_3$ ) and tri (o-tolyl)phosphine in chlorobenzene (CB) (See supplementary information for the detailed synthesis).

After the reaction, the polymers were precipitated in methanol and further purified using Soxhlet extractions with methanol, acetone, hexane, and chloroform. The polymers exhibited good solubility in common solvents like chloroform, chlorobenzene, and 1,2-dichlorobenzene. The number average molecular weights ( $M_n$ ) of **P1**, **P2** and **P3** were evaluated by gel permeation chromatography (GPC) against polystyrene standards found to be 31.1, 22.4 and 44.7 kDa with polydispersity indexes (PDI) of 3.5, 3.3 and 3.2, respectively. The thermal degradation behavior of the polymers was studied by thermal gravimetric analysis (TGA). The polymers **P1**, **P2**, and **P3** showed good thermal stability with decomposition temperatures ( $T_d$ ) of 362, 387, and 390 °C, respectively, at a 5% weight loss (Figure S1).

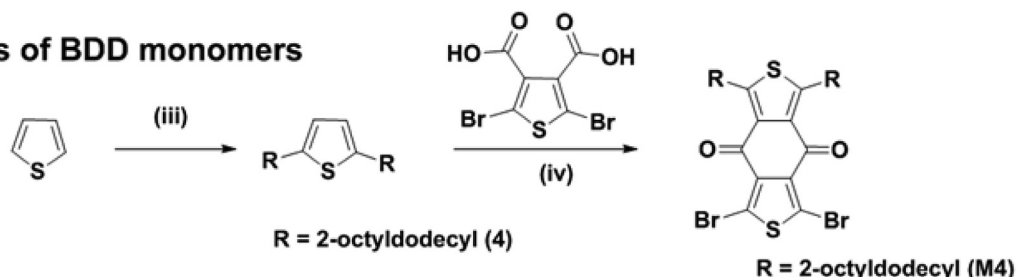


Scheme 1. Chemical structures of the three PBDD-TnFBT-based terpolymers.

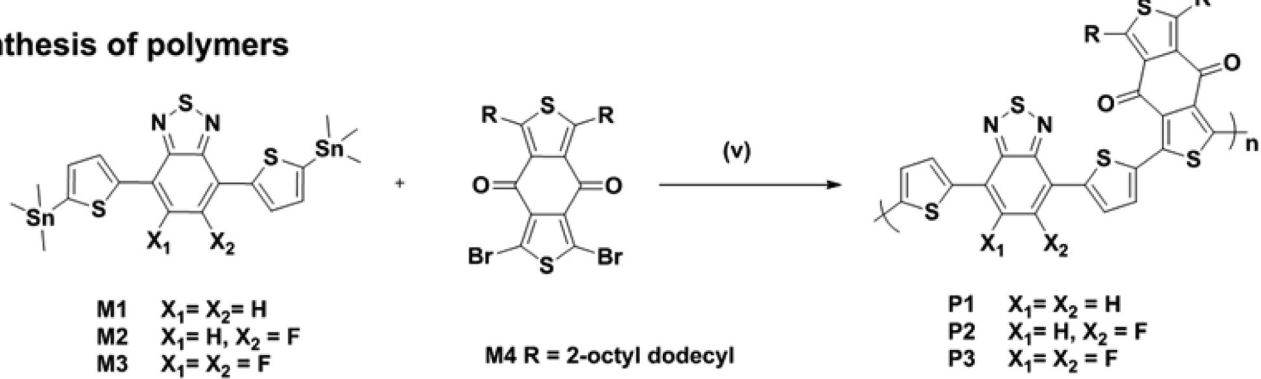
### (a) Synthesis of BT monomers



### (b) Synthesis of BDD monomers



### (c) Synthesis of polymers



**Scheme 2.** Synthetic route for monomers and polymers. (i) 2-Tributylstannylthiophene,  $\text{Pd}_2(\text{dba})_3$ , tris(*o*-tolyl)phosphine, toluene, reflux 24 h; (ii) LDA,  $-78^\circ\text{C}$ , THF, 1 h, then  $(\text{CH}_3)_3\text{SnCl}$ , RT 16 h; (iii) *n*-butyl lithium,  $0^\circ\text{C}$ , 2 h at  $50^\circ\text{C}$ , then 2-octyl dodecyl bromide, refluxed overnight; (iv) 2,5-dibromothiophene-3,4-dicarboxylic acid, oxalyl chloride, DCM, RT overnight, DCM,  $\text{AlCl}_3$ ,  $0^\circ\text{C}$ , 2,5-bis(2-octyldodecyl)thiophene, 1 h and (v)  $\text{Pd}_2(\text{dba})_3$ , tris(*o*-tolyl)phosphine, chlorobenzene, microwave.

#### 2.2. Theoretical calculations using density functional theory (DFT)

To estimate the molecular geometry and effect of fluorination on the properties of our terpolymers, we first determined their torsion angle and energy levels, and theoretically calculated their molecular structures using Gaussian 09 at B3LYP/6-31G (d) level. For simplicity, the DFT calculations were performed on two repeating units and the alkyl chain was reduced to a methyl chain (Fig. 1 and Table S1). As shown in Fig. 1a, the dihedral torsion angle between BT and its adjacent thiophene ( $\theta_1$ ) decreases as the number of F-groups on BT increased (7.7, 1.8, and  $1.3^\circ$ , respectively for **P1**, **P2**, and **P3**, respectively). In contrast, all polymers presented a torsion angle of  $\sim 21^\circ$  between BDD and thiophene ( $\theta_2$  and  $\theta_3$ ) due to the steric hindrance of the electron-withdrawing carbonyl group on the BDD. These trends indicate that drafting F substituents on BT will help diminish the steric hindrance via non-covalent conformational locks between F and S and improve molecular packing/planarity and charge transfer [31,35,36]. Moreover, fluorination of BT also decreases the C–C bond length between BT and its adjacent

thiophene in both **P2** and **P3** as shown in Fig. 1a ( $L_{\text{bond}}$  for **P1** = 145.78,  $L_{\text{bond}}$  for **P2** = 145.67, and  $L_{\text{bond}}$  for **P3** = 145.66 p.m.). Thus, fluorination increases double bond characteristics, which improves effective conjugation and structural planarity [35]. Evidently, **P3** exhibited the greatest planarity among the polymers, which is beneficial for effective stacking of polymer chains in the film state. The frontier orbitals, HOMO and lowest unoccupied molecular orbital (LUMO) energy levels of these polymers are summarized in Fig. 1b. The introduction of F atoms, ascribed to their strong electron-withdrawing ability, gradually decreased both HOMO and LUMO energy levels. These results agree with the experimental results.

#### 2.3. Optical and electrochemical properties

The normalized ultraviolet–visible (UV–vis) absorption spectra of **P1**, **P2**, and **P3** in chloroform (CF) solution and thin film states are shown in Fig. 2a and b, respectively. All terpolymers showed broad ( $\sim 300$ – $750$  nm) and characteristic dual absorption bands with

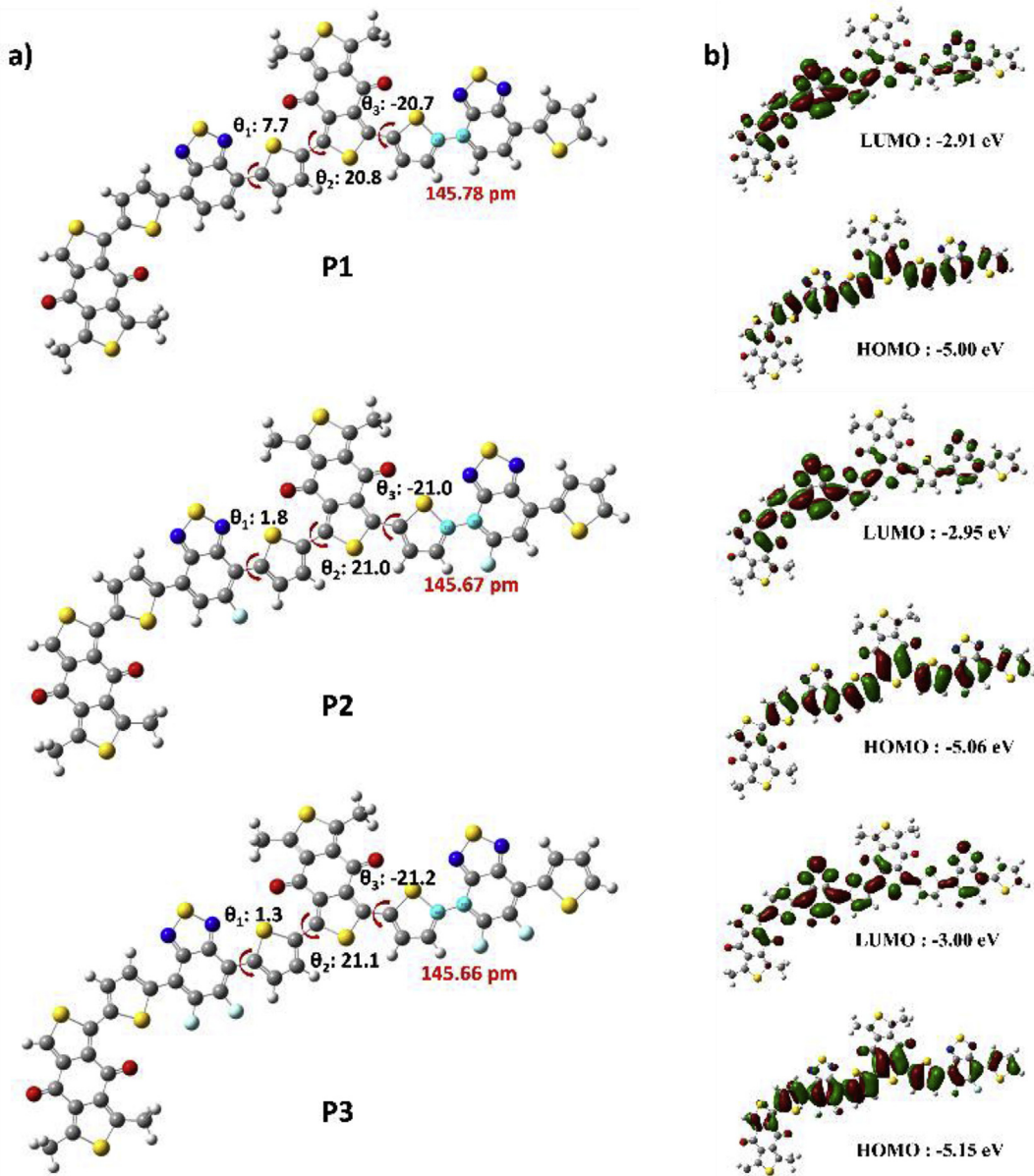


**Fig. 1.** a) The optimized molecular geometries and b) frontier molecular orbitals of **P1**, **P2**, and **P3** in dimer state. (Note: In real state, F substitution in **P2** could be random).

lower and higher energy bands originating from localized  $\pi-\pi^*$  transitions and ICT interaction, respectively [35,42]. Compared to that in solution, absorption spectra of the polymers in film state were red-shifted around  $\sim 30$  nm arising from the strong intermolecular interactions in the film state [42,43]. As the number of F substituents increased from **P1** to **P3**, corresponding absorption onset ( $\lambda_{\text{onset}}$ ) of polymers were gradually blue-shifted in both solution and film state. This is attributed to the strong electron-withdrawing tendency of the F-group, which shifts  $\pi$ -electrons and weakens conjugation [34,43]. Interestingly, **P2** showed broadened absorption profile in both solution and film compared to **P1** and **P3**. This may be caused by lower molecular weight and regiorandom structures of **P2**, resulting in their poor  $\pi-\pi$  stacking and intermolecular interactions between the polymer chains [44–47]. The **P1**, **P2**, and **P3** spectra showed absorption maxima ( $\lambda_{\text{abs}}$ ) at 627, 601, and 608 nm in CF solution and at 624, 611, and 661 nm in thin films, respectively. Among the spectra, the **P3**

spectrum displayed a pronounced vibronic peak at 661 nm in both the solution and film state, attributed to enhanced planarity and stronger stacking between the polymer chains. The molar absorptivity coefficient ( $\epsilon$ ) of the polymers were determined from Figure S2 using the Beer-Lambert law ( $A = \epsilon bc$ ),  $\epsilon$  was calculated to be 24701, 23516 and 44032  $M^{-1} \text{ cm}^{-1}$  at 600 nm for polymers **P1**, **P2** and **P3**, respectively. It is notable that higher molar absorptivity of **P3** benefits light harvesting and  $J_{\text{SC}}$  in PSC devices. Based on the  $\lambda_{\text{onset}}$  of the polymers in the film states, corresponding optical bandgaps were estimated to be 1.68, 1.70, and 1.73 eV for **P1**, **P2**, and **P3**, respectively. The complete data of optical properties of the polymers are summarized in Table 1.

As reported previously, the introduction of F atoms on the polymer backbone lead to lower HOMO and LUMO energy levels due to its strong electronegativity, which affects the  $\pi$ -orbitals in the polymers [31,34–36]. Therefore, the HOMO/LUMO energy levels of **P1**, **P2**, and **P3** determined from the corresponding cyclic

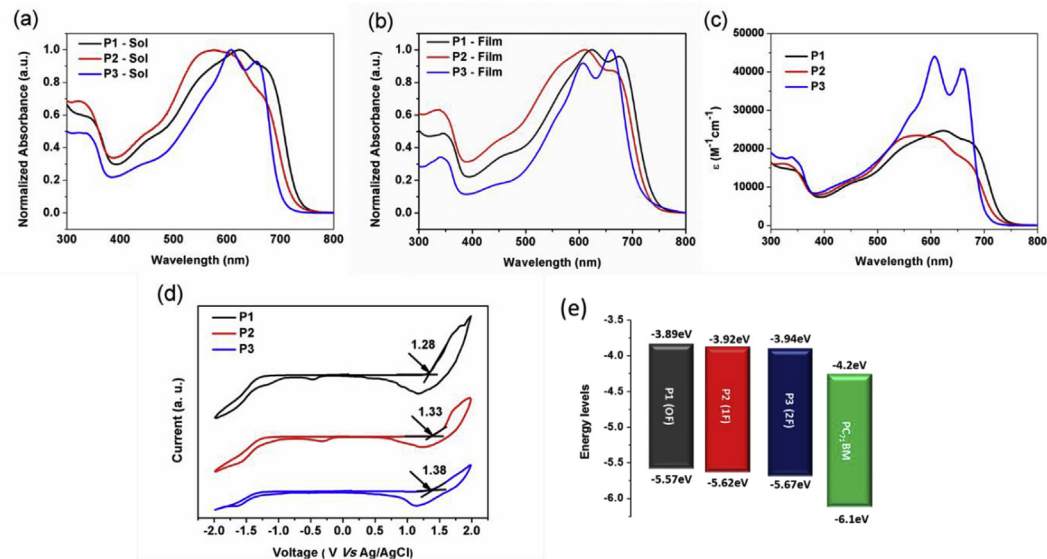


**Fig. 2.** Absorption spectra of the polymers in (a) chloroform (CF) solution, (b) thin films, (c) molar extinction coefficient ( $\epsilon$ ), (d) Cyclic voltammograms and (e) schematic energy level diagram of the polymers.

**Table 1**

Thermal, optical, and electrochemical properties of the polymers.

Polymer	Mn [kDa]/ PDI <sup>a</sup>	Thermal properties $T_d$ [ $^{\circ}$ C] <sup>b</sup>	Optical properties					Electrochemical properties	
			$\lambda_{\text{max}}$ [nm] solution	$\epsilon \times 10^4$ $\text{M}^{-1}\text{cm}^{-1}$ <sup>c</sup>	$\lambda_{\text{max}}$ [nm] film	$\lambda_{\text{onset}}$ [nm] film	$E_g^{\text{opt}}$ [eV] <sup>d</sup>	HOMO [eV]	LUMO [eV] <sup>e</sup>
<b>P1</b>	31.1/3.5	362	627	2.47	624	740	1.68	-5.57	-3.89
<b>P2</b>	22.4/3.3	387	601	2.35	611	726	1.70	-5.62	-3.92
<b>P3</b>	44.7/3.2	390	608	4.40	661	718	1.73	-5.67	-3.94

<sup>a</sup> Molecular weight determined by gel permeation chromatography (GPC).

<sup>b</sup> Decomposition temperature ( $T_d$ ) was determined by TGA (with 5% weight loss).

<sup>c</sup> The molar extinction coefficient of polymers in chloroform solution.

<sup>d</sup> Estimated values from the UV-vis absorption edge of the thin film ( $E_g^{\text{opt}} = 1240/\lambda_{\text{onset}}$  eV).

<sup>e</sup> Calculated from HOMO energy levels and optical band gap (LUMO =  $E_g^{\text{opt}} - \text{HOMO}$ ).

voltammetry (CV) and optical bandgap of the films were found to be  $-5.57$  and  $-3.89$ ,  $-5.62$  and  $-3.92$ , and  $-5.67$  and  $-3.94$  eV, respectively (Fig. 2d and e). Thus, fluorinated polymers **P2** and **P3** are expected to yield higher  $V_{\text{OC}}$  and improved oxidative stability owing to their deep HOMO energy levels. These results indicate that the substitution of F atoms in the polymer backbone is an effective strategy to modulate the intermolecular interactions and frontier energy levels of the terpolymers.

#### 2.4. Photovoltaic properties

To evaluate the effect of fluorination on photovoltaic properties of the terpolymers, PSC devices with inverted structure (indium tin oxide (ITO)/zinc oxide (ZnO)/active layer/Mo<sub>3</sub>O<sub>7</sub>/Ag) were fabricated. To achieve maximum PCE, PSC devices of each polymer were optimized by modifying its polymer to [6,6]-phenyl C<sub>71</sub> butyric acid methyl ester (PC<sub>71</sub>BM) blend ratio, spin coating speed, polymer concentration, and solvent additives. The current density-voltage ( $J-V$ ) curves and corresponding photovoltaic parameters of the optimized PSCs measured under AM 1.5 G illumination with an intensity of 100 mW/cm<sup>2</sup> are shown in Fig. 3 and Table 2, respectively, whereas detailed thickness scanning of the polymers is given in Figure S3 and Table S2. The polymers **P1**, **P2**, and **P3** performed best under optimized blend ratios of 1:1, 1:1, and 1:0.8 in CB and 3 vol% 1,8-diiodooctane (DIO), respectively. We used solvent additive DIO since it can easily solvate the PC<sub>71</sub>BM leading to

optimal BHJ morphology and higher  $J_{\text{SC}}$  in PSC devices [48,49]. As seen in Table 2, the increase in the number of fluorine atoms on the BT unit, resulted in improved PCEs. The maximum PCE were obtained at 1.4, 1.7 and 6.2% for polymers **P1**, **P2**, and **P3**, respectively. Polymers **P2** and **P3** with F substituents demonstrated higher  $V_{\text{OC}}$ , consistent with their lower HOMO energy levels. Among the polymers, **P3**:PC<sub>71</sub>BM exhibited the highest PCE of 6.2% with photovoltaic parameters  $J_{\text{SC}} = 9.00$  mA/cm<sup>2</sup>,  $V_{\text{OC}} = 1.00$  V, and fill factor (FF) = 68% (Fig. 3a). This enhancement was resulted from the improvement in photovoltaic parameters  $J_{\text{SC}}$  and  $V_{\text{OC}}$ . Figures S4–S6 and Table S3–S5 show the detailed optimization of **P3** by varying **P3**:PC<sub>71</sub>BM blend ratios, volume of the DIO additive, and device architecture. PSC devices with **P1** and **P2** displayed poor PCE, mainly due to their lower  $J_{\text{SC}}$ . It is well known that the  $J_{\text{SC}}$  of PSCs is dependent on several factors such as photocurrent generation density, molecular orientation, morphology, charge-carrier mobility, and nanoscale BHJ morphology.

Firstly, we analyzed the external quantum efficiency (EQE) spectra of the polymers to understand the reason for the significant discrepancy in their  $J_{\text{SC}}$  as shown in Fig. 3b. The  $J_{\text{SC}}$  values calculated from EQE were consistent with the experimental  $J-V$  measurements. The PSCs fabricated with **P3**:PC<sub>71</sub>BM showed significantly higher EQE values in the regions ranging from 400 to 700 nm with maximum EQE value of 50% at 640 nm. In contrast, the EQE responses of the devices based on **P1** and **P2** blends were considerably reduced to <15%, indicating poor charge separation and

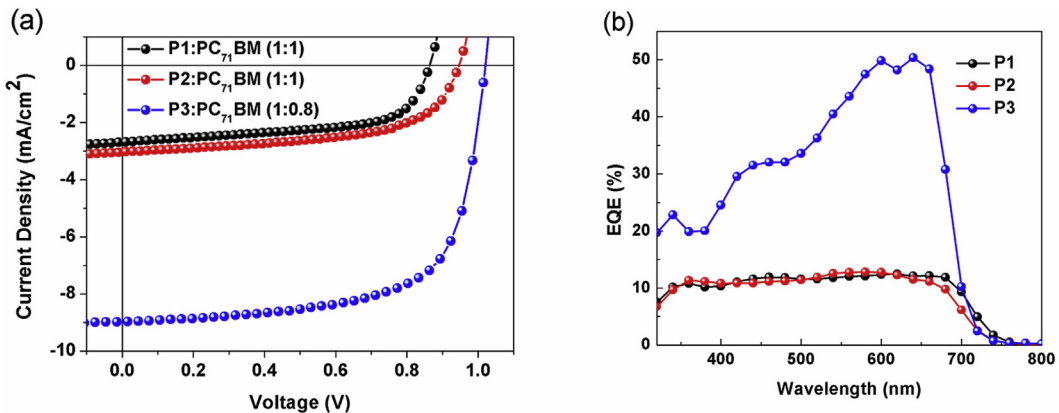


**Fig. 3.** *J-V* curves under the illumination of AM 1.5G, 100 mW cm<sup>-2</sup> for (a) **P1**, **P2** (polymer:PC<sub>71</sub>BM (1:1)) and **P3**:PC<sub>71</sub>BM (1:0.8), and (b) corresponding EQE profiles of polymers under inverted device fabrication conditions processed with CB/3 vol% DIO.

**Table 2**

Photovoltaic performance of polymer:PC<sub>71</sub>BM devices processed in CB/3 vol% DIO under the illumination of AM 1.5G, 100 mW cm<sup>-2</sup>.

Polymer	Thickness	Polymer:PC <sub>71</sub> BM	V <sub>oc</sub> [V]	J <sub>sc</sub> [mA/cm <sup>2</sup> ]	FF [%]	PCE <sup>a</sup> (PCE <sub>max</sub> )[%]	μ <sub>h</sub> [cm <sup>2</sup> /V s] <sup>b</sup>
<b>P1</b>	~80 nm	1:1	0.86 ± 0.02	2.55 ± 0.05	60.3 ± 0.2	1.33 (1.4)	3.67 × 10 <sup>-3</sup>
<b>P2</b>	~80 nm	1:1	0.93 ± 0.01	2.96 ± 0.04	57.8 ± 0.6	1.55 (1.7)	1.86 × 10 <sup>-3</sup>
<b>P3</b>	~100 nm	1:0.8	0.99 ± 0.01	8.96 ± 0.04	67.6 ± 0.4	5.97 (6.2)	4.92 × 10 <sup>-3</sup>

The devices architecture is ITO/ZnO/active layer/MoO<sub>3</sub>/Ag.

<sup>a</sup> The average PCE values and standard deviation are based on over 8 independent devices.

<sup>b</sup> Hole-only device is ITO/PEDOT:PSS/Active Layer/MoO<sub>3</sub>/Ag.

transport. This accords with the *J<sub>sc</sub>* values of the polymer devices. Thus, higher molar absorptivity of **P3** is one of the factors that contributed to enhancing the *J<sub>sc</sub>* in devices through effective photocurrent generation.

## 2.5. Molecular packing

Factors such as crystallinity and molecular orientation greatly determine the charge-transport characteristics of PSCs [31,36]. Hence, we compared the bulk morphology of pristine polymers and polymer:PC<sub>71</sub>BM blend films via XRD analysis (Fig. 4). Table S6 enlists the corresponding packing parameters extracted from the XRD results. All polymers in pristine film state showed pronounced (100), (200), and (010) diffraction peaks in the out-of-plane direction ( $q_z$ ) (Fig. 4a) and (010) peaks in the in-plane directions ( $q_{xy}$ ) (Fig. 4b), indicating the existence of bimodal edge-on and face-on orientations. Moreover,  $\pi-\pi$  stacking distances in both out-of-plane and in-plane directions decreased with increasing number of F substituents (3.56/3.51 Å for **P1** to 3.52/3.49 Å for **P2** and 3.51/3.48 Å for **P3**, respectively). These results indicate that the introduction of F atoms in the polymer backbone assists in the formation of compact polymer crystallites via stronger interchain packing as reported previously [31,35–37]. Evidently, fluorinated polymers **P2** and **P3** have higher crystallinity than nonfluorinated polymer **P1**.

In the blend films, the (100) diffraction peaks in the  $q_z$ -plane for **P1**:PC<sub>71</sub>BM and **P3**:PC<sub>71</sub>BM vanished (Fig. 4c) but remained for **P2**:PC<sub>71</sub>BM (3.22 Å<sup>-1</sup>, d = 27.42 Å). However, all the polymer blends retained their (010) Bragg's diffraction peaks in  $q_z$ -plane (Fig. 4c) with corresponding  $\pi-\pi$  stacking distances of 3.58 Å, 3.54 Å and 3.51 Å for **P1**, **P2**, and **P3**, respectively. Consequently, **P1**:PC<sub>71</sub>BM and **P3**:PC<sub>71</sub>BM blend films exhibited preferential face-on orientations in contrast with **P2**:PC<sub>71</sub>BM which showed mixed orientation. Furthermore,  $\pi-\pi$  stacking distances of **P1**:PC<sub>71</sub>BM (3.56–3.58 Å) and **P2**:PC<sub>71</sub>BM (3.52–3.54 Å) blends increased after

mixing with PC<sub>71</sub>BM, whereas that of **P3**:PC<sub>71</sub>BM (3.51–3.51 Å) was unchanged. These trends indicate possible polymer aggregation in **P1** and **P2** blend films (consistent with AFM morphology images). Overall, face-on molecular orientation and shorter  $\pi-\pi$  stacking distances in **P3**:PC<sub>71</sub>BM benefits vertical charge transport in PSC devices [23,31,50], in comparison with **P2**:PC<sub>71</sub>BM.

## 2.6. Hole mobility

To elucidate the effect of fluorination on the charge transport properties of the polymers, we measured the hole mobility of the pristine polymers and polymer:PC<sub>71</sub>BM blend using space-charge-limited current (SCLC) method [51]. The fabricated hole-only devices having the structure of ITO/PEDOT:PSS/active layer/MoO<sub>3</sub>/Ag and corresponding plots of dark current versus voltage are shown in Figure S7. The hole mobilities of the pristine polymers were in the order of  $6.84 \times 10^{-3}$ ,  $5.09 \times 10^{-3}$  and  $3.30 \times 10^{-3}$  cm<sup>2</sup>/V for the **P3**, **P1** and **P2**, respectively. In this series, **P3** exhibited highest hole mobility correlated well with its higher crystallinity and compact molecular packing. The high hole mobility will prevent accumulation of charges and decreases charge recombination, thus boosting *J<sub>sc</sub>* and efficiency [42,53,54]. However, **P2** displayed lower mobility compared with the zero F-constituent counterpart **P1**. This may be ascribed from the lower molecular weight of **P2**, which confines their conjugation length, thereby resulting in lower photocurrent densities and poor interconnectivity of the polymer chains as reported previously [45,52]. In the blend films, hole mobility trend was like that of pristine polymers i.e.  $4.92 \times 10^{-3}$  (**P3**) >  $3.67 \times 10^{-3}$  (**P1**) and  $>1.86 \times 10^{-3}$  cm<sup>2</sup>/V (**P2**). Thus, higher hole mobility in **P3**:PC<sub>71</sub>BM blends can be explained by the enhanced co-planarity and interchain ordering facilitated two fluorine substituents, which further assisted the formation of the highly ordered face-on molecular orientation with shorter  $\pi-\pi$  stacking distances as revealed in XRD studies. As a result, high hole mobilities of the

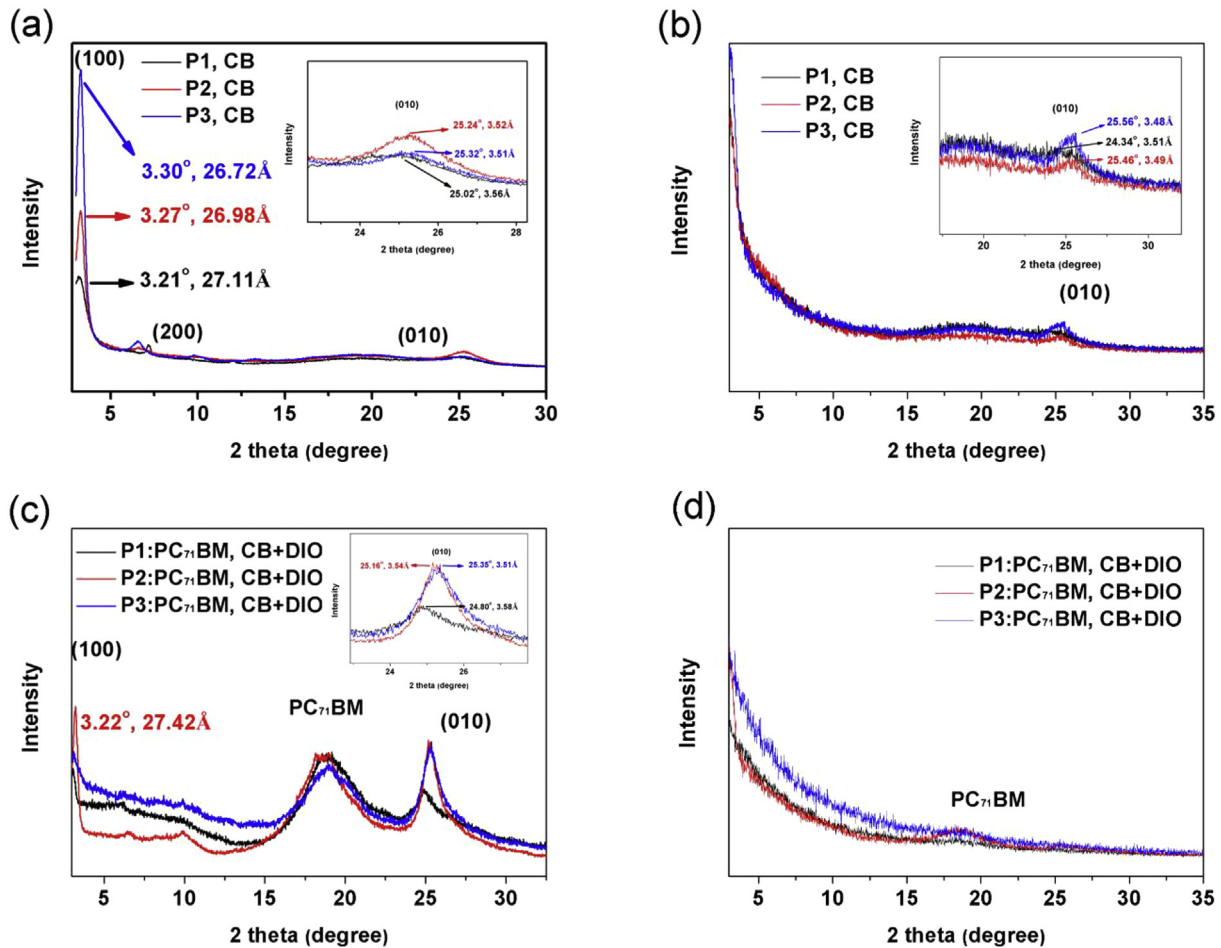


**Fig. 4.** (A, c) Out-of-plane ( $q_z$ ) and (b, d) in-plane ( $q_{xy}$ ) line cut profiles of the XRD images obtained from pristine polymers and polymer:PC<sub>71</sub>BM blends, respectively.

**P3:PC<sub>71</sub>BM** blends leading to higher  $J_{SC}$ , FF, and efficiency in associated PSCs.

## 2.7. Nanoscale film morphology

The nanoscale morphology of the polymer:PC<sub>71</sub>BM blends greatly affect exciton dissociation and charge transport in the PSCs. Therefore, we analyzed the surface morphology of our polymer blends using atomic force microscopy (AFM) in tapping-mode ( $5\text{ }\mu\text{m} \times 5\text{ }\mu\text{m}$ ) to examine their effects on the photovoltaic properties (Fig. 5). As shown in the AFM height images, polymer:PC<sub>71</sub>BM film blends of **P1** (Fig. 5a and d) and **P2** (Fig. 5b and e) displayed rougher morphologies with large, aggregated domains over 200 nm, indicating phase segregation. In contrast, **P3** blend exhibited a much smoother and uniform BHJ morphology with distinct miscible P3 and PC<sub>71</sub>BM phases of smaller domain size (Fig. 5c and f). The root mean square (RMS) roughness of the blends decreased in the order of **P1** (11.32 nm) > **P2** (10.49 nm) and > **P3** (3.48 nm). According to previous studies about high-efficiency polymers, uniform BHJ morphology with bicontinuous fibrillar interpenetrating network of 10–20 nm domain sizes are beneficial for efficient exciton dissociation and charge transports in the PSCs [8,31,40], whereas larger phase separation will reduce D-A interfacial area, hence hindering them [48,54]. Moreover, some reports showed polymer:fullerene miscibility, morphology evolution and the performances are closely related with the fluorine content in the conjugated polymer [43,55,56]. Particularly, Lee et al. and Liu

et al. reported the decrease in the polymer:fullerene phase segregation with higher F-contents due to the reduction of the solubility of the fluorinated polymers favoring decreased fibril size [55,56]. Additionally, some recent studies by Yan, Hou, Ade and co-workers demonstrated the direct quantitative relations between interaction parameter, miscibility and photovoltaic performances in both fullerene and non-fullerene systems. They emphasized the importance of achieving high purity and ordered packing at smaller length scale (~10 nm) are necessary for enhancing the FF/ $J_{SC}$  in PSCs [57,58]. Thus, favorable nanoscale morphology with uniform and smaller domain sizes in **P3** blend is arising from the presence of two F-substituents, which greatly improved polymer miscibility with PC<sub>71</sub>BM and decreased the size of the phase separation.

Overall, lower molar absorptivity and inferior nanoscale morphology in **P1** and **P2** devices negatively affecting the overall light harvesting, charge separation and collection in the devices, hence affecting their photovoltaic performances. Thus, several positive factors of **P3** blends such as high molar absorptivity, compact  $\pi-\pi$  stacking, high hole mobility, and optimum nanoscale morphology greatly contributed to improved  $J_{SC}$ , FF, and efficiency. These AFM results agree with the XRD data and expected photovoltaic properties.

## 3. Conclusion

In conclusion, we successfully synthesized three PBDD-TnFBT ( $n = 0, 1, 2$ ) terpolymers with the varying number of F atoms on

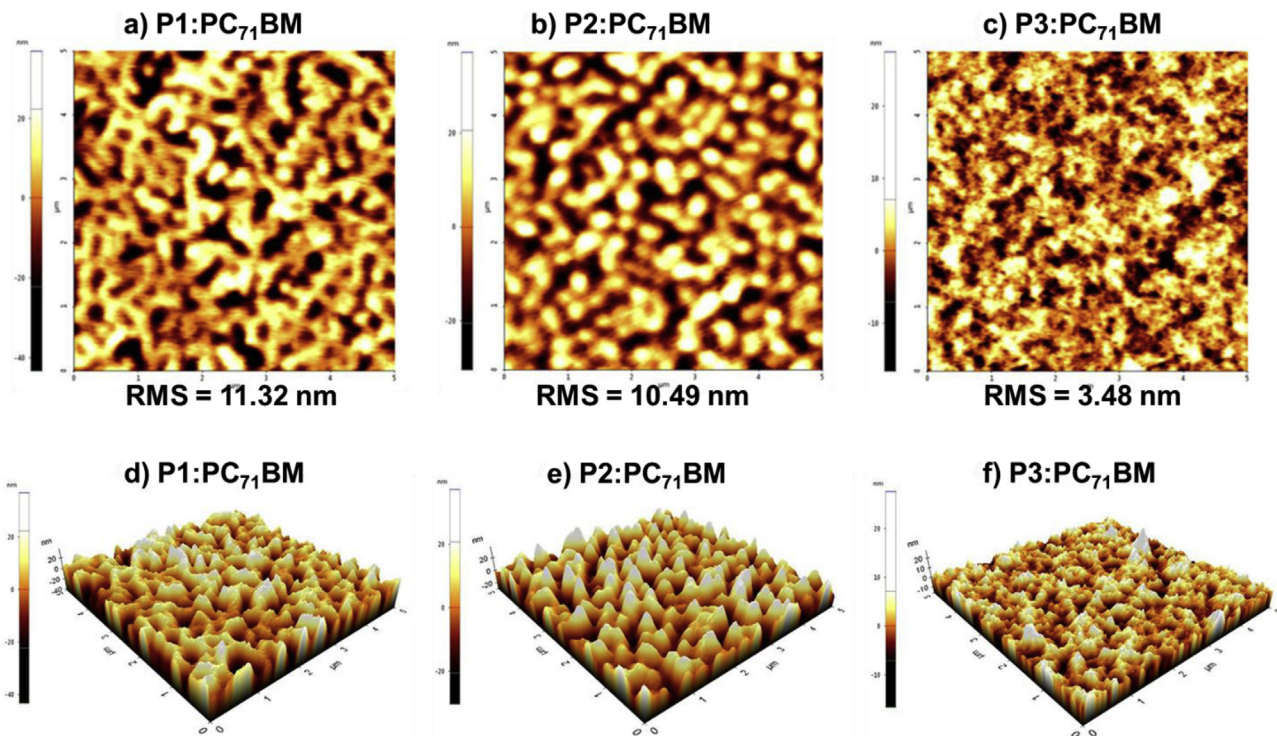


**Fig. 5.** AFM height (top) and 3-D topography images (bottom) of the **P1:PC<sub>71</sub>BM** (a and d), **P2:PC<sub>71</sub>BM** (b and e) and **P3:PC<sub>71</sub>BM** (c and f) processed under optimized device fabrication conditions.

BT. The effect of F substitution was also evaluated by investigating the basic optoelectronic properties, molecular orientation, and photovoltaic performance of the terpolymers. They covered broad absorption range (~750 nm) due to effective ICT interactions of the two different acceptors (BT and BDD) and thiophene donor. Increasing the number of F atom on the BT unit lowered the frontier molecular orbitals, improved the molecular planarity and intermolecular interaction between neighboring polymers chains. The polymer **P3**, having 2 F substituents on BT, displayed good miscibility with PC<sub>71</sub>BM, a predominant face-on molecular orientation, and optimal nanoscale morphology. As a result, PSCs devices based on **P3** had the best photovoltaic performance with a PCE of 6.2%. This study illustrates the interrelation between the degree of fluorination with intermolecular interactions, charge transport behavior, BHJ morphology, and polymer performance in PSC and effectively contributes to designing efficient polymer donors for photovoltaic application.

## Acknowledgements

This research was supported by the New & Renewable Energy Core Technology Program (No. 20153010140030) and Human Resources program in Energy Technology (No. 20174010201540) of the Korea Institute of Energy Technology Evaluation and Planning grant funded by the Ministry of Trade, Industry & Energy, Republic of Korea. This research was supported by the 2018 KU Brain Pool of Konkuk University.

## Appendix A. Supplementary data

Supplementary data related to this article can be found at <https://doi.org/10.1016/j.polymer.2018.06.038>.

## References

- [1] C.J. Brabec, Organic photovoltaics: technology and market, *Sol. Energy Mater. Sol. Cells* 83 (2004) 273–292.
- [2] F.C. Krebs, Fabrication and processing of polymer solar cells: a review of printing and coating techniques, *Sol. Energy Mater. Sol. Cells* 93 (2009) 394–412.
- [3] A.C. Arias, J.D. MacKenzie, I. McCulloch, J. Rivnay, A. Salleo, Materials and applications for large area electronics: solution-based approaches, *Chem. Rev.* 110 (2010) 3–24.
- [4] T.D. Nielsen, C. Cruickshank, S. Foged, J. Thorsen, F.C. Krebs, Business, market and intellectual property analysis of polymer solar cells, *Sol. Energy Mater. Sol. Cells* 94 (2010) 1553–1571.
- [5] G. Li, R. Zhu, Y. Yang, Polymer solar cells, *Nat. Photon.* 6 (2012) 153–161.
- [6] Y. Liu, J. Zhao, Z. Li, C. Mu, Wei Ma, H. Hu, K. Jiang, H. Lin, H. Ade, H. Yan, Aggregation and morphology control enables multiple cases of high-efficiency polymer solar cells, *Nat. Commun.* 5 (2014) 5293.
- [7] J. Zhao, Y. Li, Y. Guofang, K. Jiang, H. Lin, H. Ade, Wei Ma, H. Yan, Efficient organic solar cells processed from hydrocarbon solvents, *Nature Energy* 1 (2016) 15027.
- [8] Y. Jin, Z. Chen, M. Xiao, J. Peng, B. Fan, L. Ying, G. Zhang, X.-F. Jiang, Q. Yin, Z. Liang, F. Huang, Y. Cao, Thick film polymer solar cells based on naphtho[1,2-c:5,6-c']bis[1,2,5-thiadiazole conjugated polymers with efficiency over 11%, *Adv. Energy Mater.* 7 (2017), 1700944.
- [9] W. Li, J. Cai, F. Cai, Y. Yan, H. Yi, R.S. Gurney, et al., Achieving over 11% power conversion efficiency in PffBT4T-2OD-based ternary polymer solar cells with enhanced open-circuit-voltage and suppressed charge recombination, *Nanomater. Energy* 44 (2018) 155–163.
- [10] W. Zhao, S. Li, H. Yao, S. Zhang, Y. Zhang, B. Yang, Jianhui Hou, Molecular optimization enables over 13% efficiency in organic solar cells, *J. Am. Chem. Soc.* 139 (2017) 7148–7151.
- [11] X. Xu, T. Yu, Z. Bi, W. Ma, Y. Li, Q. Peng, Realizing over 13% Efficiency in green-solvent-processed nonfullerene organic solar cells enabled by 1,3,4-thiadiazole-based wide-bandgap copolymers, *Adv. Mater.* 30 (2017), 1703973.
- [12] C. Sun, F. Pan, H. Bin, J. Zhang, L. Xue, B. Qiu, Z. Wei, Z.-G. Zhang, Y.F. Li, A low cost and high performance polymer donor material for polymer solar cells, *Nat. Commun.* 9 (2018) 743.
- [13] L. Ye, Y. Xiong, Q. Zhang, S. Li, C. Wang, Z. Jiang, J. Hou, W. You, H. Ade, Surpassing 10% efficiency benchmark for nonfullerene organic solar cells by scalable coating in air from single nonhalogenated solvent, *Adv. Mater.* 30 (2018), 1705485.
- [14] J. Sun, X. Ma, Z. Zhang, J. Yu, J. Zhou, X. Yin, L. Yang, R. Geng, R. Zhu, F. Zhang, W. Tang, Dithieno[3,2-b:2',3'-d]pyrrol fused nonfullerene acceptors enabling

- over 13% efficiency for organic solar cells, *Adv. Mater.* (2018), 1707150.
- [15] M.L. Keshtov, A.R. Khokhlov, S.A. Kuklin, F.C. Chen, A.Y. Nikolaev, E.N. Koukaras, G.D. Sharma, Synthesis of alternating D–A1–D–A2 terpolymers comprising two electron-deficient moieties, quinoxaline and benzothiadiazole units for photovoltaic applications, *Polym. Chem.* 7 (2016) 4025–4035.
- [16] Z. Deng, F. Wu, L. Chen, Y. Chen, Novel photovoltaic donor 1–acceptor–donor 2–acceptor terpolymers with tunable energy levels based on a difluorinated benzothiadiazole acceptor, *RSC Adv.* 5 (2015) 12087–12093.
- [17] T.E. Kang, K.-H. Kim, B.J. Kim, Design of terpolymers as electron donors for highly efficient polymer solar cells, *J. Mater. Chem. A* 2 (2014) 15252–15267.
- [18] W. Sun, Z. Ma, D. Dang, W. Zhu, M. Andersson, F. Zhang, An alternating D–A1–D–A2 copolymer containing two electron-deficient moieties for efficient polymer solar cells, *J. Mater. Chem. A* 1 (2013) 11141–11144.
- [19] M.L. Keshtov, A.R. Khokhlov, S.A. Kuklin, F.C. Chen, E.N. Koukaras, G.D. Sharma, New D-A1-D-A2-type regular terpolymers containing benzothiadiazole and benzotriphosphine acceptor units for photovoltaic application, *ACS Appl. Mater. Interfaces* 8 (2016) 32998–33009.
- [20] T. Ma, K. Jiang, S. Chen, H. Hu, H. Lin, Z. Li, J. Zhao, Y. Liu, Y.-M. Chang, C.-C. Hsiao, H. Yan, Efficient low-bandgap polymer solar cells with high open-circuit voltage and good stability, *Adv. Energy Mater.* 5 (2015), 1501282.
- [21] Q. Tao, Y. Xia, X. Xu, S. Hedstrom, O. Backe, D.I. James, P. Persson, E. Olsson, O. Inganäs, L. Hou, W. Zhu, E. Wang, D–A<sub>1</sub>–D–A<sub>2</sub> copolymers with extended donor segments for efficient polymer solar cells, *Macromolecules* 48 (2015) 1009–1016.
- [22] B. Fan, X. Xue, X. Meng, X. Sun, L. Huo, W. Ma, Y. Sun, High-performance conjugated terpolymer-based organic bulk heterojunction solar cells, *J. Mater. Chem. A* 4 (2016) 13930–13937.
- [23] G.P. Kini, Q.V. Hoang, C.E. Song, S.K. Lee, W.S. Shin, W.-W. So, M.A. Uddin, H.Y. Woo, J.-C. Lee, Thiophene-benzothiadiazole based D–A1–D–A2 type alternating copolymers for polymer solar cells, *Polym. Chem.* 8 (2017) 3622–3631.
- [24] T. Jiang, J. Yang, Y. Tao, C. Fan, L. Xue, Z. Zhang, H. Li, Y. Li, Wei Huang, Random terpolymer with a cost-effective monomer and comparable efficiency to PTB7-Th for bulk-heterojunction polymer solar cells, *Polym. Chem.* 7 (2016) 926–932.
- [25] D.P. Qian, L. Ye, M.J. Zhang, Y.R. Liang, L.J. Li, Y. Huang, X. Guo, S.Q. Zhang, Z.A. Tan, J.H. Hou, Design, application, and morphology study of a new photovoltaic polymer with strong aggregation in solution state, *Macromolecules* 45 (2012) 9611–9617.
- [26] H. Zhang, Y. Liu, Y. Sun, M. Li, B. Kan, X. Ke, Q. Zhang, X. Wan, Y. Chen, Developing high-performance small molecule organic solar cells via a large planar structure and an electron-withdrawing central unit, *Chem. Commun.* 53 (2017) 451–454.
- [27] L. Huo, T. Liu, X. Sun, Y. Cai, A.J. Heeger, Y. Sun, Single-junction organic solar cells based on a novel wide-bandgap polymer with efficiency of 9.7%, *Adv. Mater.* 27 (2015) 2938.
- [28] Q. Fan, W. Su, X. Guo, B. Guo, W. Li, Y. Zhang, K. Wang, M. Zhang, Y. Li, A new polythiophene derivative for high efficiency polymer solar cells with PCE over 9%, *Energy Mater.* 6 (2016), 1600430.
- [29] X. Huang, K. Weng, L. Huo, B. Fan, C. Yang, X. Sunb, Y. Sun, Effects of a heteroatomic benzothienothiophenedione acceptor on the properties of a series of wide-bandgap photovoltaic polymers, *J. Mater. Chem. C* 4 (2016) 9052–9059.
- [30] T. Liu, X. Pan, X. Meng, Y. Liu, D. Wei, W. Ma, L.J. Huo, X. Sun, T.H. Lee, M. Huang, H. Choi, J.Y. Kim, W.C.H. Choy, Y.M. Sun, Alkyl side-chain engineering in wide-bandgap copolymers leading to power conversion efficiencies over 10%, *Adv. Mater.* 29 (2017), 1604251.
- [31] T.L. Nguyen, H. Choi, S.-J. Ko, M.A. Uddin, B. Walker, S. Yum, J.-E. Jeong, M.H. Yun, T.J. Shin, S. Hwang, J.Y. Kim, H.Y. Woo, Semi-crystalline photovoltaic polymers with efficiency exceeding 9% in a ~300 nm thick conventional single-cell device, *Energy Environ. Sci.* 7 (2014) 3040–3051.
- [32] Y. Wang, T. Michinobu, Benzothiadiazole and its  $\pi$ -extended, heteroannulated derivatives: useful acceptor building blocks for high-performance donor–acceptor polymers in organic electronics, *J. Mater. Chem. C* 4 (2016) 6200–6214.
- [33] Q. Zhang, M.A. Kelly, N. Bauer, W. You, The curious case of fluorination of conjugated polymers for solar cells, *Acc. Chem. Res.* 50 (2017) 2401–2409.
- [34] W.T. Neo, K.H. Ong, T.T. Lin, S.-J. Chuac, J. Xu, Effects of fluorination on the electrochromic performance of benzothiadiazole-based donor–acceptor copolymers, *J. Mater. Chem. C* 3 (2015) 5589–5597.
- [35] J. Hwang, J. Park, Y.J. Kim, Y.H. Ha, C.E. Park, D.S. Chung, S.-K. Kwon, Y.-H. Kim, Indolo[3,2-*b*]indole-containing donor–acceptor copolymers for high-efficiency organic solar cells, *Chem. Mater.* 29 (2017) 2135–2140.
- [36] I.-B. Kim, S.-Y. Jang, Y.-A. Kim, R. Kang, I.-S. Kim, D.-K. Ko, D.-Y. Kim, The effect of fluorine substitution on the molecular interactions and performance in polymer solar cells, *ACS Appl. Mater. Interfaces* 9 (2017) 24011–24019.
- [37] Z. Hu, H. Chen, J. Qu, X. Zhong, P. Chao, M. Xie, W. Lu, A. Liu, L. Tian, Y.-A. Su, W. Chen, F. He, Design and synthesis of chlorinated benzothiadiazole-based polymers for efficient solar energy conversion, *ACS Energy Lett.* 2 (2017) 753–758.
- [38] D. Mo, H. Wang, H. Chen, S. Qu, P. Chao, Z. Yang, L. Tian, Y.A. Su, Y. Gao, B. Yang, W. Chen, F. He, Chlorination of low-band-gap polymers: toward high-performance polymer solar cells, *Chem. Mater.* 29 (2017) 2819–2830.
- [39] S.-H. Kang, G.D. Tabi, J. Lee, G. Kim, Y.-Y. Noh, C. Yang, Chlorinated 2,1,3-benzothiadiazole-based polymers for organic field-effect transistors, *Macromolecules* 50 (2017) 4649–4657.
- [40] G.P. Kini, S.K. Lee, W.S. Shin, S.-J. Moon, C.E. Song, J.-C. Lee, Achieving a solar power conversion efficiency exceeding 9% by modifying the structure of a simple, inexpensive and highly scalable polymer, *J. Mater. Chem. A* 4 (2016) 18585–18597.
- [41] A. Casey, Y. Han, Z. Fei, A.J.P. White, T.D. Anthopoulos, M. Heeney, Cyanobenzothiadiazole: a novel acceptor inducing n-type behaviour in conjugated polymers, *J. Mater. Chem. C* 3 (2015) 265–275.
- [42] C.E. Song, Y.J. Kim, S.R. Suranagi, G.P. Kini, S. Park, S.K. Lee, W.S. Shin, S.-J. Moon, I.-N. Kang, C.E. Park, J.-C. Lee, Impact of the crystalline packing structures on charge transport and recombination via alkyl chain tunability of DPP-based small molecules in bulk heterojunction solar cells, *ACS Appl. Mater. Interfaces* (2016) 12940–12950.
- [43] G. Liu, C. Weng, P. Yin, S. Tan, P. Shen, Impact of the number of fluorine atoms on crystalline, physicochemical and photovoltaic properties of low bandgap copolymers based on 1,4-dithienylphenylene and diketopyrrolopyrrole, *Polymer* 125 (2017) 217–226.
- [44] S. Hayashi, S. Yamamoto, T. Koizumi, Effects of molecular weight on the optical and electrochemical properties of EDOT-based  $\pi$ -conjugated polymers, *Sci. Rep.* 7 (2017) 1078.
- [45] Z. Xiao, K. Sun, J. Subbiah, T. Qin, S. Lu, B. Purushothaman, D.J. Jones, A.B. Homes, W.W.H. Wong, Effect of molecular weight on the properties and organic solar cell device performance of a donor–acceptor conjugated polymer, *Polym. Chem.* 6 (2015) 2312–2318.
- [46] J. Yuan, M.J. Ford, Y. Zhang, H. Dong, Z. Li, Y. Li, T.-Q. Nguyen, G.C. Bhajan, W. Ma, Toward thermal stable and high photovoltaic efficiency ternary conjugated copolymers: influence of backbone fluorination and regioselectivity, *Chem. Mater.* 29 (2017) 1758–1768.
- [47] K.H. Hendriks, G.H.L. Heintges, M.M. Wienk, R.A.J. Janssen, Comparing random and regular diketopyrrolopyrrole–bithiophene–thienopyrrolodione terpolymers for organic photovoltaics, *J. Mater. Chem. A* 2 (2014) 17899.
- [48] H.-C. Liao, C.-C. Ho, C.-Y. Chang, M.-H. Jao, S.B. Darling, W.-F. Su, Additives for morphology control in high-efficiency organic solar cells, *Material today* 16 (2013), 326–326.
- [49] A. Zusan, B. Giesecking, M. Zerson, V. Dyakonov, R. Magerle, C. Deibel, The effect of diiodooctane on the charge carrier generation in organic solar cells based on the copolymer PBDTTT-C, *Sci. Rep.* 5 (2015) 8286.
- [50] V. Vohra, K. Kawashima, T. Kakara, T. Koganezawa, I. Osaka, K. Takimiya, H. Murata, Efficient inverted polymer solar cells employing favourable molecular orientation, *Nat. Photon.* 9 (2015) 403–408.
- [51] G.G. Malliaras, J.R. Salem, P.J. Brock, C. Scott, Electrical characteristics and efficiency of single-layer organic light-emitting diodes, *Phys. Rev. B* 58 (1998). R13411.
- [52] C. Liu, K. Wang, X. Hu, Y. Yang, C.-H. Hsu, W. Zhang, S. Xiao, X. Gong, Y. Cao, Molecular weight effect on the efficiency of polymer solar cells, *ACS Appl. Mater. Interfaces* 5 (2013) 12163–12167.
- [53] Y. Jin, Z. Chen, S. Dong, N. Zheng, L. Ying, X.-F. Jiang, F. Liu, F. Huang, Y. Cao, A Novel Naphtho[1,2-c:5,6-c']bis([1,2,5]thiadiazole)-based narrow-bandgap  $\pi$ -conjugated polymer with power conversion efficiency over 10%, *Adv. Materials* 28 (2016) 9811–9818.
- [54] G.P. Kini, S. Oh, Z. Abbas, S. Rasool, M. Jahandar, C.E. Song, S.K. Lee, W.S. Shin, W.W. So, J.C. Lee, Effects on photovoltaic performance of dialkylxybenzothiadiazole copolymers by varying the thienoacene donor, *ACS Appl. Mater. Interfaces* 9 (2017) 12617–12628.
- [55] J.Y. Lee, J.W. Jo, W.H. Jo, Effect of fluorine substitution on photovoltaic performance of DPP-based copolymer, *Org. Electron.* 20 (2015) 125–131.
- [56] P. Liu, K. Zhang, F. Liu, Y. Jin, S. Liu, T.P. Russell, H.-L. Yip, F. Huang, Y. Cao, Effect of fluorine content in thienothiophene-benzodithiophene copolymers on the morphology and performance of polymer solar cells, *Chem. Mater.* 26 (2014) 3009–3017.
- [57] L. Ye, W. Zhao, S. Li, S. Mukherjee, J.H. Carpenter, O. Awartani, X. Jiao, J. Hou, H. Ade, High-efficiency nonfullerene organic solar cells: critical factors that affect complex multi-length scale morphology and device performance, *Adv. Energy Mater.* 7 (2017), 1602000.
- [58] L. Ye, H. Hu, M. Ghasemi, T. Wang, B.A. Collins, J.H. Kim, K. Jiang, J.-H. Carpenter, H. Li, Z. Li, T. McAfee, J. Zhao, X. Chen, J.L.Y. Lai, T. Ma, J.-L. Bredas, H. Yan, H. Ade, Quantitative relations between interaction parameter, miscibility and function in organic solar cells, *Nat. Mater.* 17 (2018) 253–260.